Supporting Information

Mechanism and Kinetics for Reaction of the Chemical Warfare Agent Simulant, DMMP(*g*), with Zirconium (IV) MOFs: An Ultrahigh-vacuum and DFT Study

G. Wang,[1] C. Sharp,[1] A. M. Plonka,[2] Q. Wang,[2] A. Frenkel,[2] W. Guo,[3] C. Hill,[3] C. Smith,[1] J. Kollar,[4] D. Troya,[1] and J. R. Morris[1,*]

[1]*Department of Chemistry, Virginia Tech, Blacksburg, Virginia 24061, United States*

[2]*Department of Materials Science and Chemical Engineering, Stony Brook University, Stony Brook, New York 11794, United States*

[3]*Department of Chemistry, Emory University, Atlanta, Georgia 30322, United States*

[4]*Department of Chemistry and Biochemistry, Kennesaw State University, Kennesaw, Georgia 30144, United States*

Corresponding Author

*jrmorris@vt.edu

Table of Contents

Section S1: Powder x-ray diffractograms of UiO-66, UiO-67, and MOF-808

The powder XRD measurements were performed with synchrotron X-rays at the 17-BM beam line at the Advanced Photon Source (APS) at Argonne National Laboratory with the fast and large 2D detector, using the beam of λ=0.72959 Å and were analyzed using GSAS-II software. The PXRD patterns of UiO-66, UiO-67 and MOF-808 are consistent with those of the ideal structures, as verified by comparison to models.

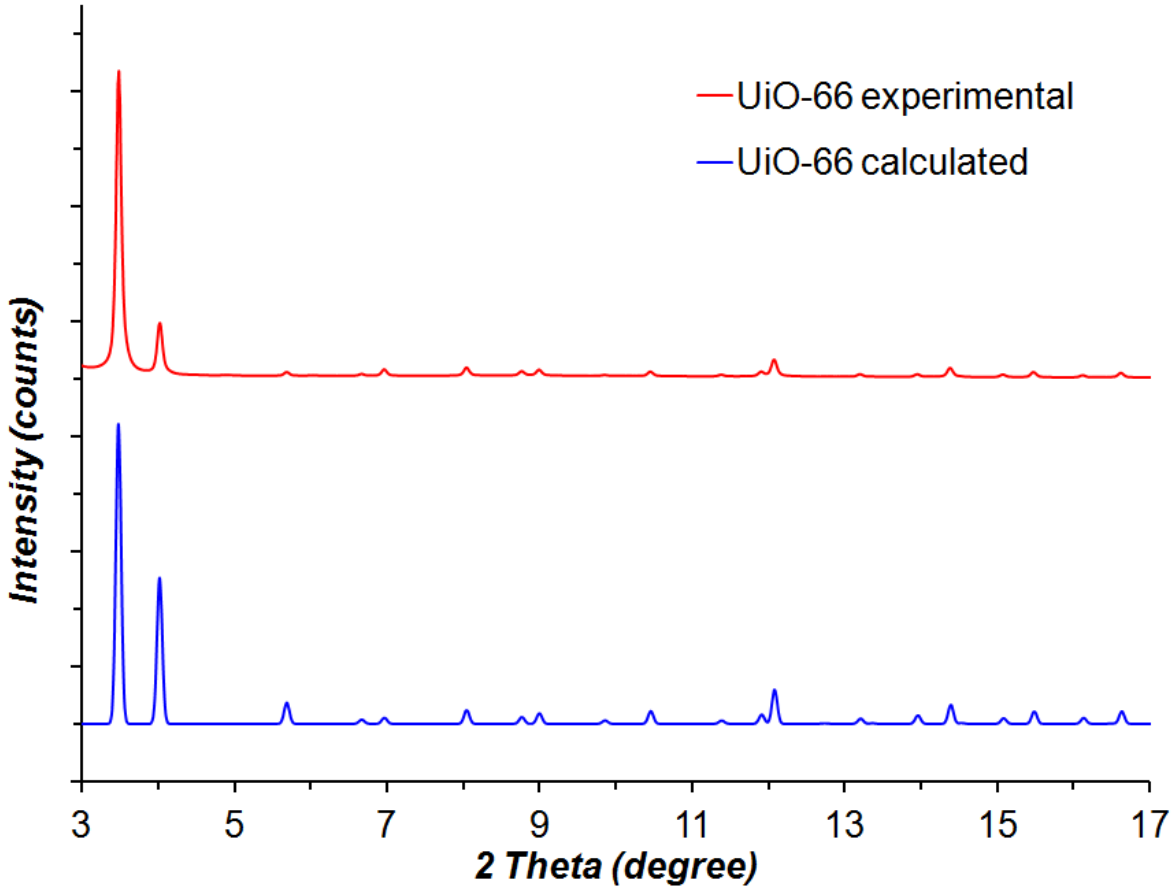

Figure S1. Experimental PXRD pattern of UiO-66 compared with the pattern calculated from the single crystal structure. No additional peaks indicate the purity of the sample.

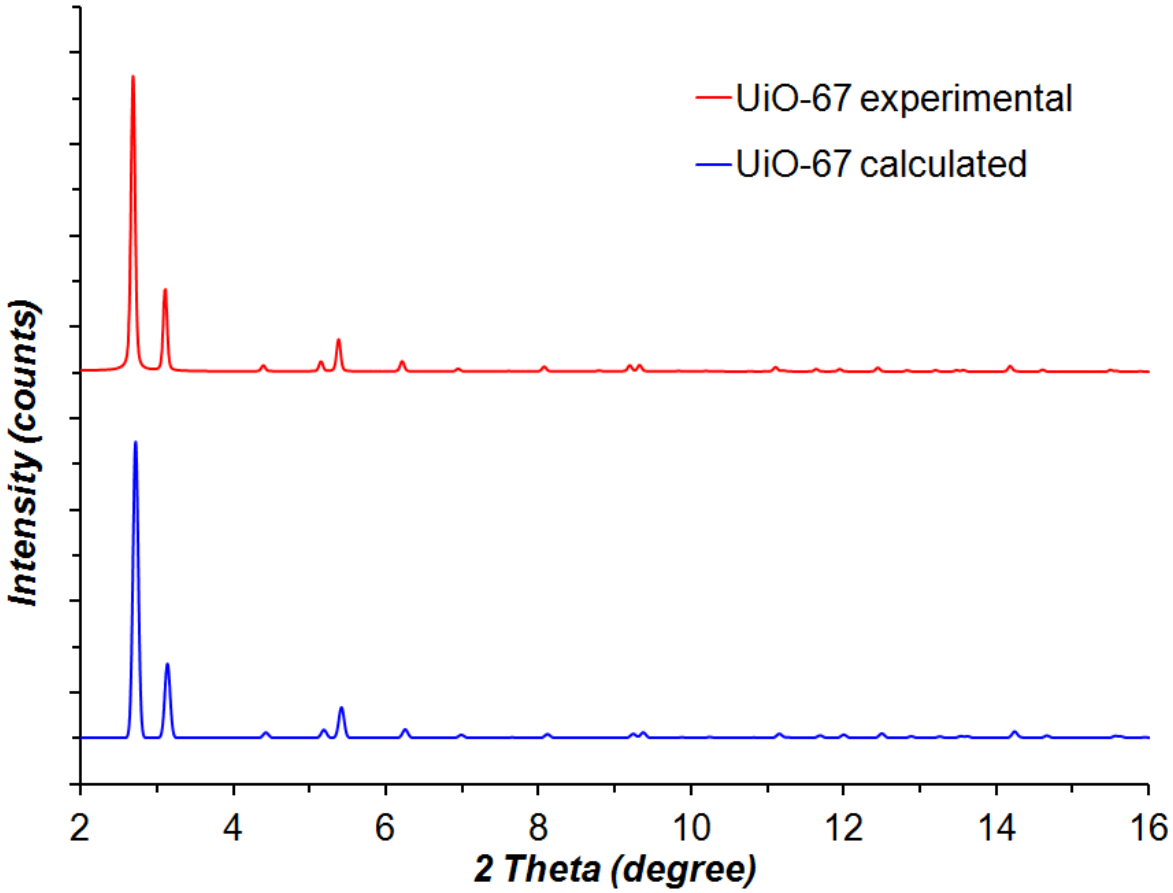

Figure S2. Experimental PXRD pattern of UiO-67 compared with the pattern calculated from the single crystal structure. No additional peaks indicate the purity of the sample.

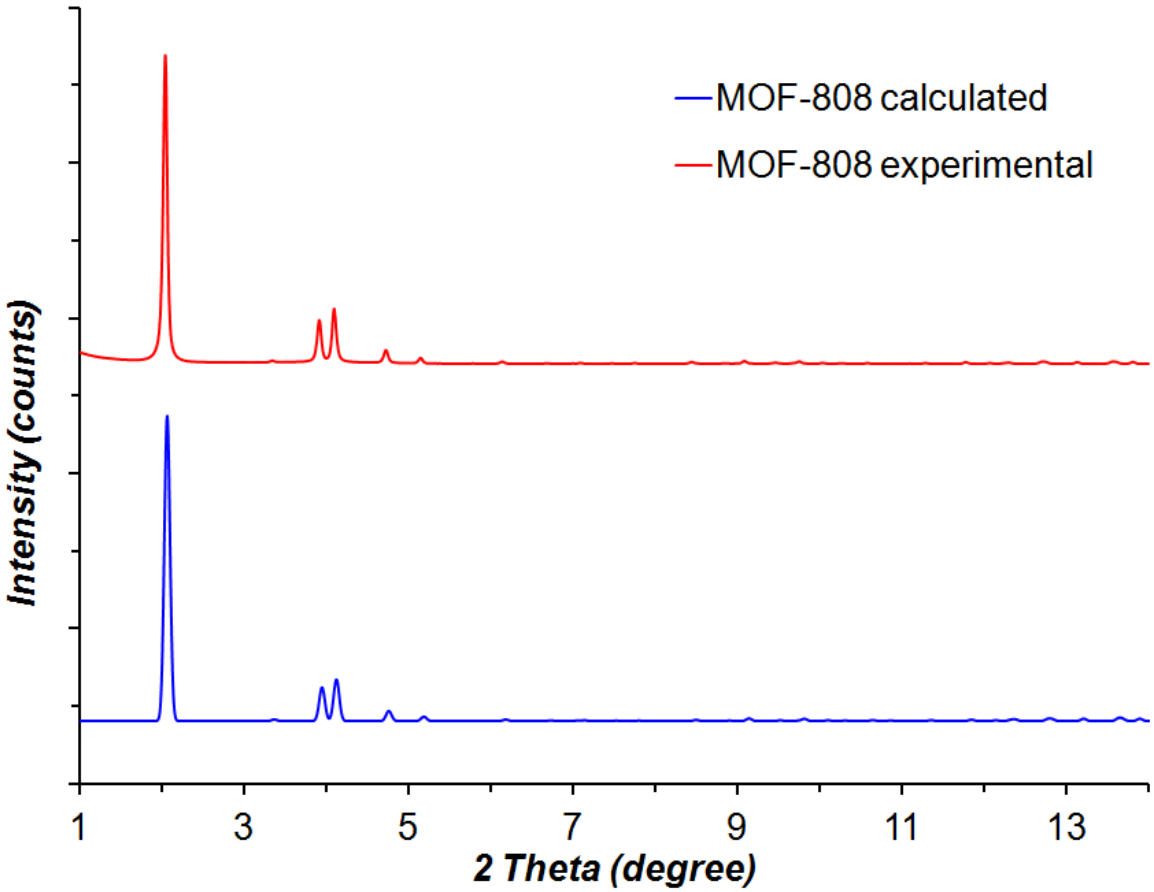

Figure S3. Experimental PXRD pattern of MOF-808 compared with the pattern calculated from the single crystal structure. No additional peaks indicate the purity of the sample.

Table S1. Unit cell parameters of UiO-66, UiO-67, MOF-808 from this study, compared with published results. Small differences in values arise from different temperatures of data collection.

MOF	this study		published	
	lattice parameter *a* (Å)	T(K)	lattice parameter *a* (Å)	T (K)
UiO-66	20.7582(6)	298	20.7465(2)*	100
UiO-67	28.845(1)	298	26.783(3)**	100
MOF-808	35.371(2)	298	35.0764(10)***	100

*[1], **[2], ***[3]

Section S2: Infrared band assignment for peaks in difference IR spectra of UiO-66, UiO-67, and MOF-808 upon DMMP exposure

The difference IR spectra of UiO-66, UiO-67, and MOF-808 were recorded by a Bruker IFS 66v/S spectrometer. The clean, pre-exposed MOFs were used as the background. The difference IR spectra of UiO-66 upon DMMP exposure can be found in Figure 3, while Figure S4 shows the difference IR pf UiO-67 (Black) and MOF-808 (Red). The assignments for the IR bands in the difference spectra are shown in Table S2.

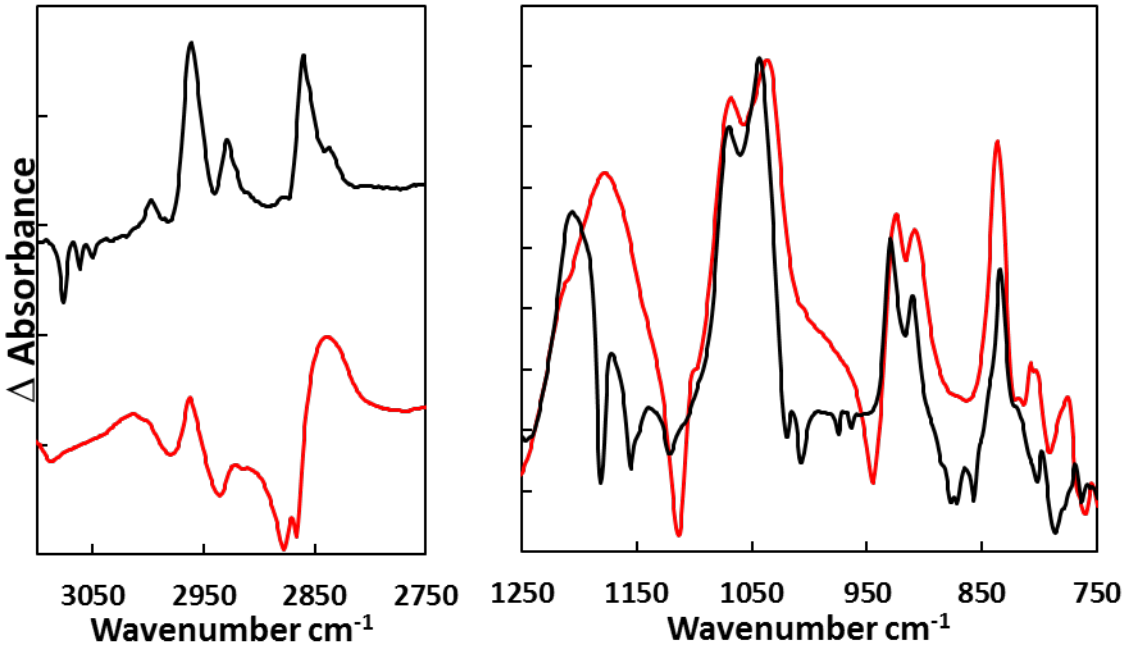

Figure S4. Difference IR spectra of MOF-808(Red) and UiO-67 (Black) upon DMMP exposure at room temperature (298 K)

Table S2. Observed vibrational frequencies (cm^{-1}) in difference IR spectra of Zr_6 MOFs upon DMMP exposure and their assignments.[4]

Mode	UiO-66-DMMP cm^{-1}	UiO-67-DMMP cm^{-1}	MOF-808-DMMP cm^{-1}
$\nu(ZrO{-}H)_{SBU,\ H\text{-}bounded}$	3313		
$\nu_{as}(CH_3)$	3009	2997	3012
$\nu_{as}(CH_3O)$	2950	2961	2962
$\nu_s(CH_3)$	2950sh	2961sh	2962sh
$\nu_{as}(ZrOCH_3)$		2928	2913
$\nu_s(CH_3O)$	2846	2860	2839
$\nu_s(ZrOCH_3)$		2836	2839sh
$\delta(PCH_3)+\delta(P=O)+\nu_{as}(O\text{-}P\text{-}O)+\rho(OCH_3)$			1178
$\delta(PCH_3)$	1308	1207	
$\upsilon(P=O)$	1255	1171	
$\nu_{as}(O\text{-}P\text{-}O)+\rho(OCH_3)$	1186	1138	
$\nu_s(O\text{-}P\text{-}O)$	1064sh	1070sh	1068sh
$\nu_{as}(CO)$	1064	1070	1068
$\nu_s(CO)$	1048	1043	1038
$\rho(PCH_3)_{P=O\ bounded\ to\ SBU}$	952	926	925
$\rho(PCH_3)$	912	910	909
$\nu(P\text{-}C)$	819	834	837
$\nu(P\text{-}O)$	789	819	775

ν: bond stretching, ρ: rocking (in plane), δ: angle bending

Section S3: DFT calculations to accompany DMMP-Zr_6 MOF overall reaction pathway calculations

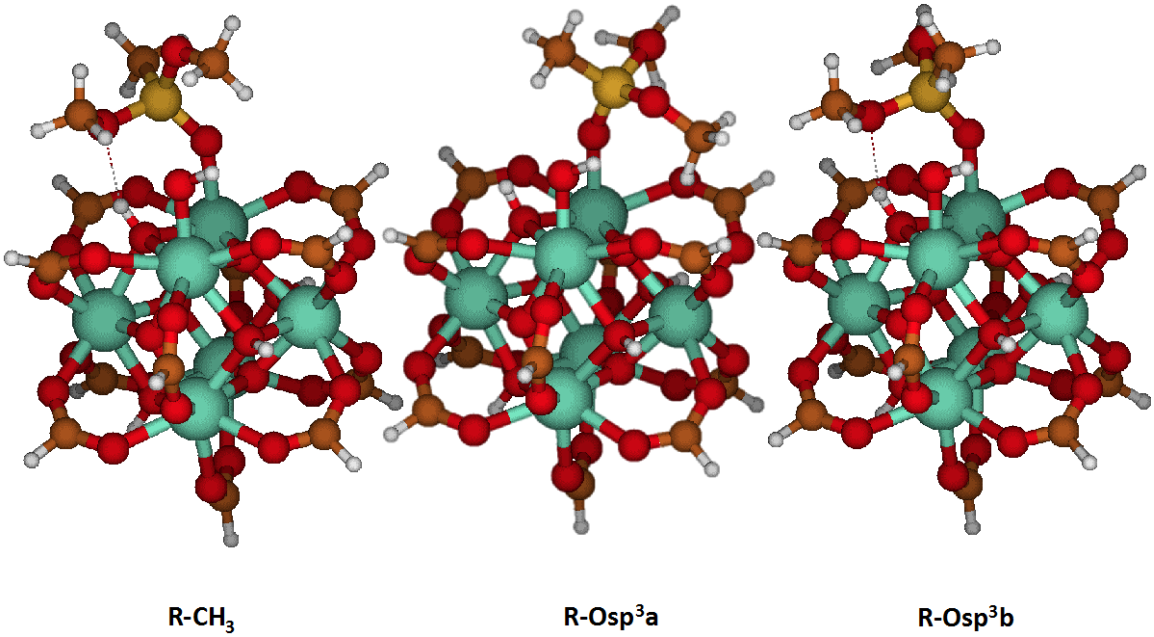

Figure S5. Three possible reactive orientations of DMMP with respect to the Zr-OH group at a missing linker defect of UiO-67. The reaction pathway for the R-CH_3 orientation is shown in Figs. 10 and 11, and those for R-Osp^3a and b are in Figs. S7-S9.

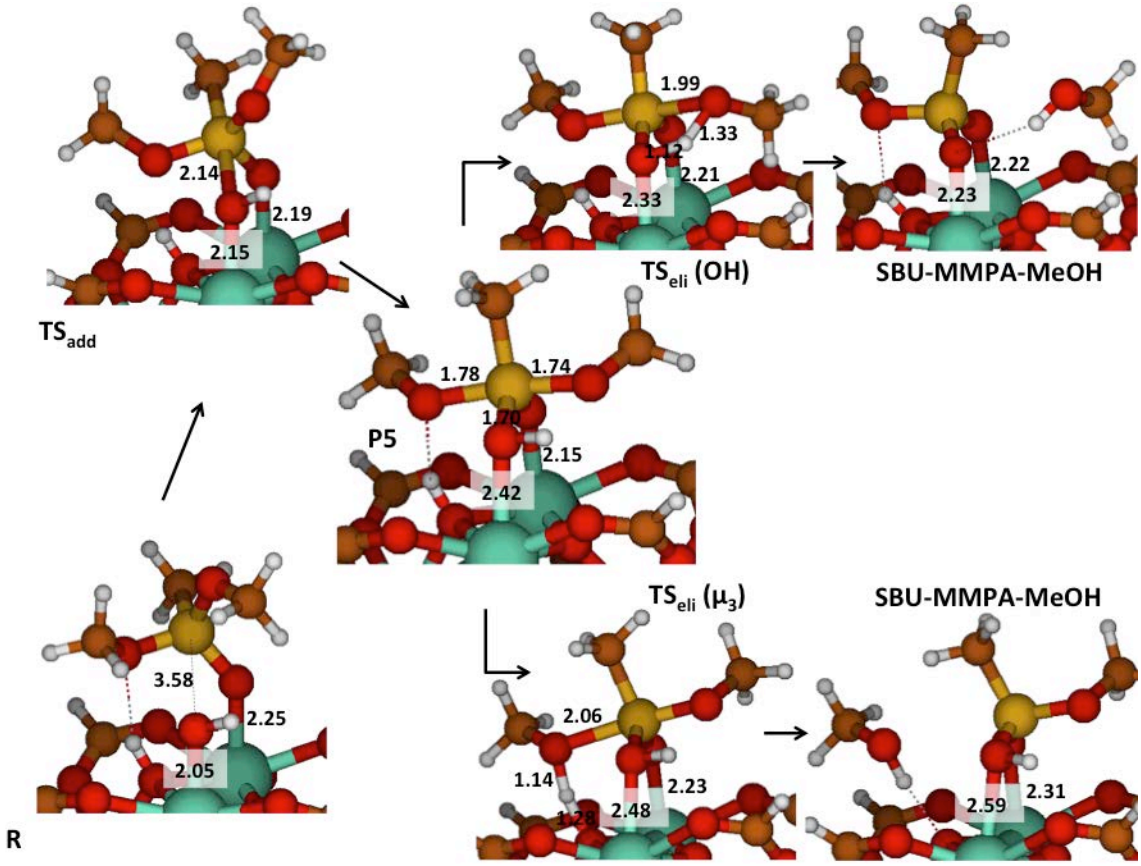

Figure S6. Selected bond distances in the central stationary points of the decomposition of DMMP with a defective SBU of UiO-67 along the approach in which the P–CH_3 bond of DMMP is collinear to the forming P–OH bond at the addition transition state. Same color code as Fig. 11.

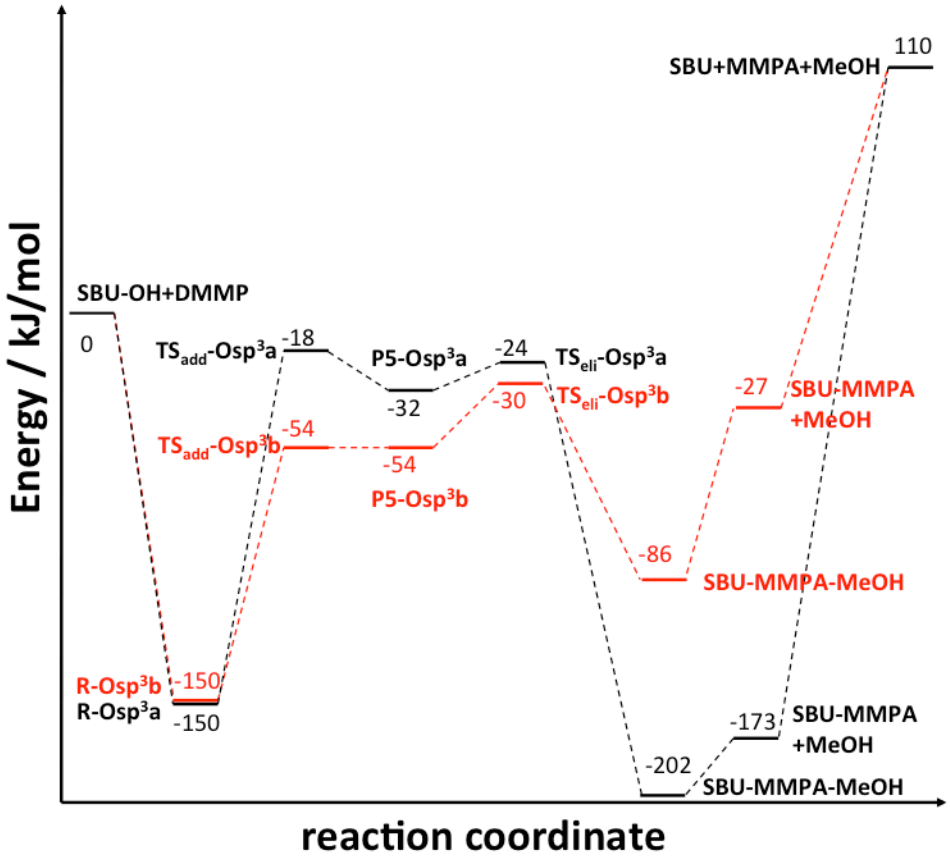

Figure S7. Potential-energy profile for the reaction of DMMP with a defective SBU of UiO-67 along the approaches in which the P–OCH_3 bond of DMMP is collinear to the forming P–OH bond at the addition transition state

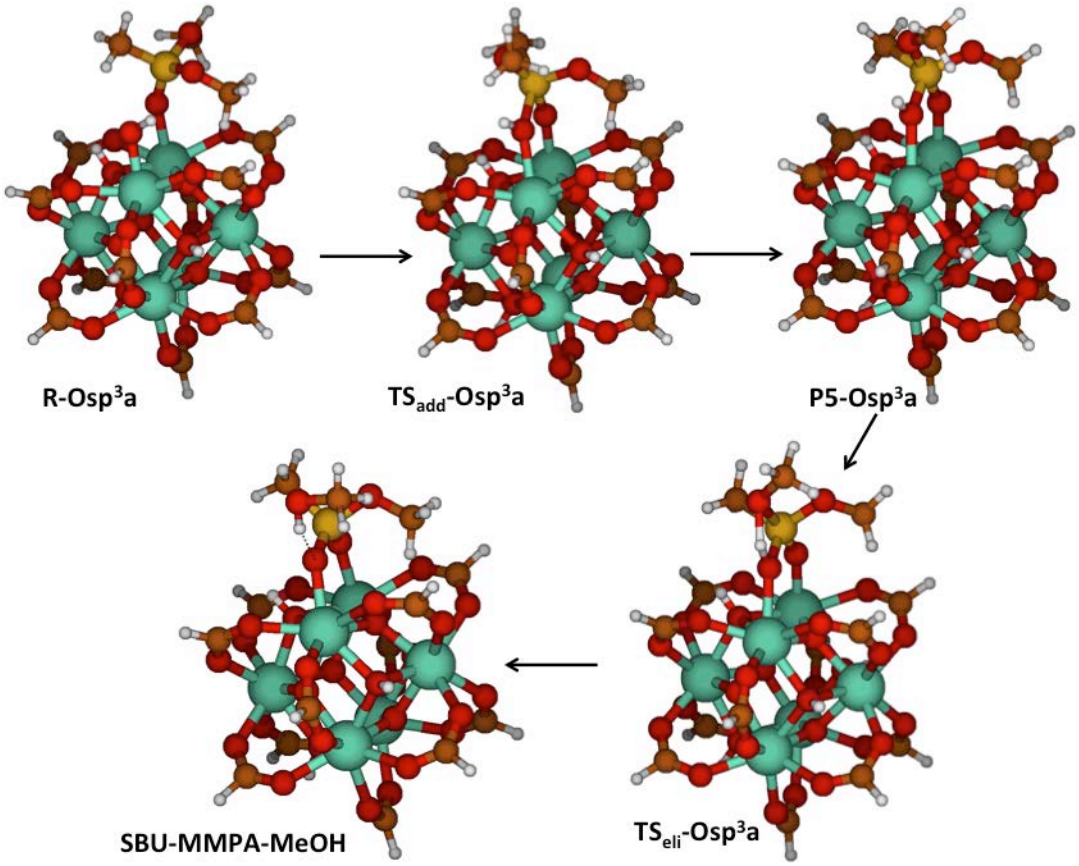

Figure S8. Geometries of the central stationary points in the decomposition of DMMP with a defective SBU of UiO-67 along the "Osp3a" approach in Fig. S7. Same color code as Fig. 11.

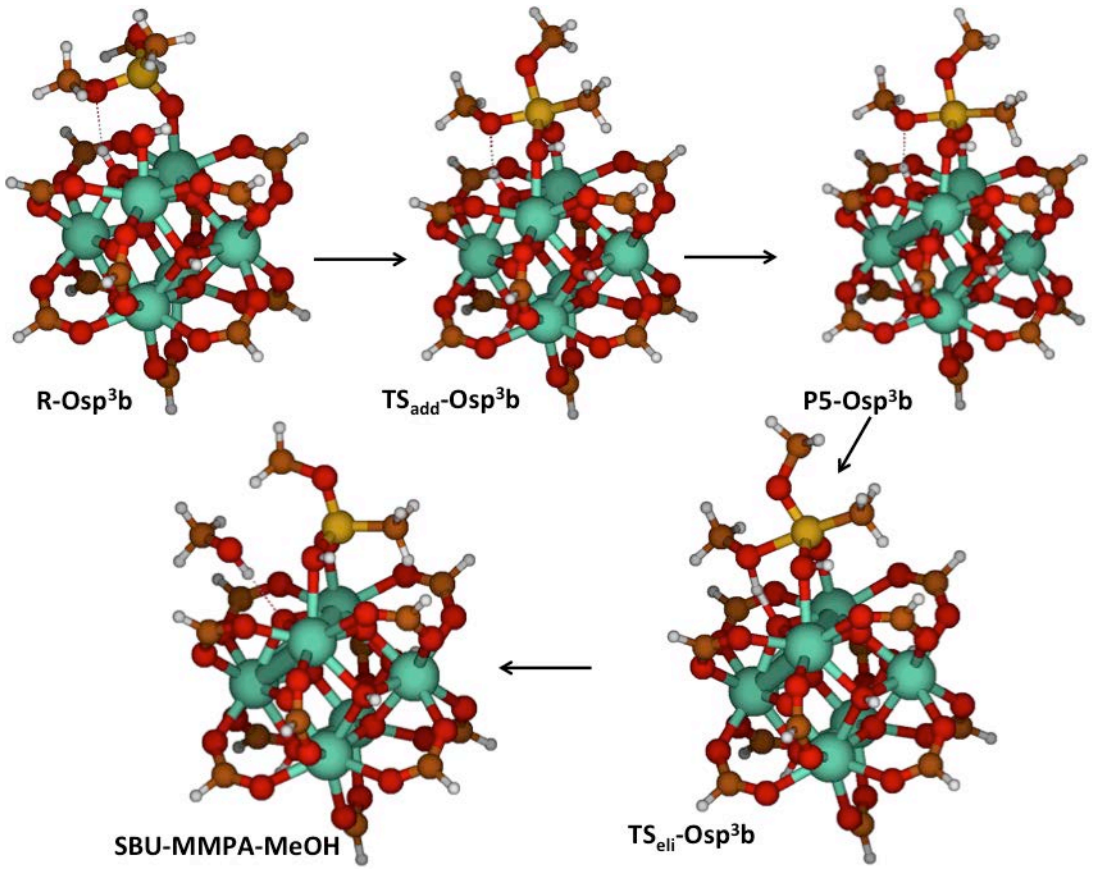

Figure S9. Geometries of the central stationary points in the decomposition of DMMP with a defective SBU of UiO-67 along the "Osp3b" approach in Fig. S7. Same color code as Fig. 11.

1. Øien, S.; Wragg, D.; Reinsch, H.; Svelle, S.; Bordiga, S.; Lamberti, C.; Lillerud, K. P., Detailed Structure Analysis of Atomic Positions and Defects in Zirconium Metal–Organic Frameworks. *Crystal Growth & Design* **2014,** *14*, 5370-5372.
2. Ko, N.; Hong, J.; Sung, S.; Cordova, K. E.; Park, H. J.; Yang, J. K.; Kim, J., A Significant Enhancement of Water Vapour Uptake at Low Pressure by Amine-Functionalization of UiO-67. *Dalton Transactions* **2015,** *44*, 2047-2051.
3. Furukawa, H.; Gandara, F.; Zhang, Y. B.; Jiang, J. C.; Queen, W. L.; Hudson, M. R.; Yaghi, O. M., Water Adsorption in Porous Metal-Organic Frameworks and Related Materials. *J. Am. Chem. Soc.* **2014,** *136*, 4369-4381.
4. Gordon, W. O.; Tissue, B. M.; Morris, J. R., Adsorption and Decomposition of Dimethyl Methylphosphonate on Y2O3 Nanoparticles. *J. Phys. Chem. C* **2007,** *111*, 3233-3240.